PHYSICAL REVIEW B **84**, 075473 (2011)

Two-photon photoluminescence excitation spectroscopy of single quantum dots

Y. Benny,* Y. Kodriano, E. Poem, S. Khatsevitch, and D. Gershoni
Physics Department and Solid State Institute, Technion–Israel Institute of Technology, Haifa 32000, Israel

P. M. Petroff
Materials Department, University of California, Santa Barbara, California 93106, USA
(Received 18 May 2011; revised manuscript received 11 July 2011; published 12 August 2011)

We present an experimental and theoretical study of single semiconductor quantum dots excited by two nondegenerate, resonantly tuned, variably polarized lasers. The first laser is tuned to excitonic resonances. Depending on its polarization it photogenerates a coherent single-exciton state. The second laser is tuned to biexciton resonances. By scanning the energy of the second laser for various polarizations of the two lasers, while monitoring the emission from the biexciton and exciton spectral lines, we map the biexciton photoluminescence excitation spectra. The resonance-rich spectra of the second photon absorption are analyzed and fully understood in terms of a many-carrier theoretical model which takes into account the direct and exchange Coulomb interactions between the quantum confined carriers.

DOI: 10.1103/PhysRevB.84.075473 PACS number(s): 78.67.Hc, 73.21.La

I. INTRODUCTION

Semiconductor quantum dots (QDs) confine charge carriers in three spatial directions. This confinement results in a discrete spectrum of energy levels and energetically sharp optical transitions between these levels.[1,2] These "atomic-like" features, together with their compatibility with modern semiconductor-based microelectronics and optoelectronics, make QDs promising building block devices for future technologies involving single-photon emitters[3] and quantum information processing (QIP).[4–6] In particular, QDs are considered to be an excellent interface between photons, whose polarization state may carry quantum information from one site to another, and confined-carriers' spins, whose states can be coherently manipulated locally.[7,8] For these reasons, it is very important to study and to understand in detail light-matter interactions in such nanostructures. Deep understanding of these interactions is required in order to implement protocols and schemes relevant to QIP[9] in these manmade, technology-compatible "artificial atoms."

In this work we present a comprehensive study of single, neutral semiconductor QDs subject to excitation by two different variably polarized resonant lasers. The first laser is tuned to an excitonic resonance and generates a coherent single-exciton state, while the second laser is scanned through biexcitonic resonances. Depending on the particular resonance and the direction of the light polarization relative to the direction of the exciton spin, it photogenerates a biexciton.[8] The absorption is then monitored through the emission intensities of various biexcitonic and excitonic spectral lines.

The manuscript is organized as follows: Section II is devoted to setting the theoretical background which is required to analyze the experimental data. In Sec. III we describe the experimental methods and the measurements that we performed. In Sec. IV we present the experimental results and analyze the data, using the theory outlined in Sec. II. The last part of this section provides a short summary of the results.

II. THEORY

We use a simple one-band model to describe the single-particle wave functions of electrons in the conduction band and heavy holes in the valence band of a single QD. Since in these InAs/GaAs lattice mismatch strain induced self-assembled QDs, the light-holes band is energetically separated from the heavy-hole band by the strain and the quantum size effect; light holes are not considered in our model. The lateral extent of these QDs is typically about an order of magnitude larger than their extent along the growth direction. Therefore, for simplicity, our model considers only the two lateral directions. The exact composition and strain distribution in these QDs are not accurately known; therefore we use a very simple, two-dimensional parabolic potential model to describe the QD influence on the carriers that it confines. This simple model is general enough to describe the C_{2v} symmetry of these QDs,[10] and it contains four parameters (see below) which permit its adjustment to the experimental observations.[2] Two separated infinite elliptic parabolic potentials are thus used, one for the electrons and one for the heavy holes.[11] The resulting envelope wave functions or orbitals of the carriers are therefore described analytically by the 2D harmonic solutions:

$$\psi^{p}_{n_x,n_y}(x,y) = \frac{H_{n_x}\left(\frac{x}{l^x_p}\right) H_{n_y}\left(\frac{y}{l^y_p}\right)}{\sqrt{2^{(n_x+n_y)} n_x! n_y! \pi l^x_p l^y_p}} \times \exp\left(\frac{1}{2}\left[\left(\frac{x}{l^x_p}\right)^2 + \left(\frac{y}{l^y_p}\right)^2\right]\right), \quad (1)$$

where $p = \mathrm{e}$ (h) stands for electron (heavy hole) and $H_{n_{x(y)}}$ are the Hermite polynomials of order $n_{x(y)}$.

$$l^{x(y)}_p = \sqrt{\frac{\hbar}{M^*_{\perp,p}\omega^{x(y)}_p}} \quad (2)$$

is a characteristic length, which describes the extent of the parabolic potential along the $x(y)$ direction, and Eq. (2) relates this length to the charge carrier's in-plane effective mass $M^*_{\perp,p}$

and the harmonic potential interlevel energy separation $\hbar\omega_p^{x(y)}$. We fit the four characteristic lengths $l_{e(h)}^{x(y)}$ to best describe the observed spectral lines.

Equipped with the single carrier's eigenenergies and envelope wave functions we proceed by calculating the many-carrier energies and states using the configuration interaction (CI) model.[2,12,13] A detailed description of the model, which takes into account the direct and exchange Coulomb interactions between any pair of carriers in the QD, is presented elsewhere.[2]

Previous studies dealt mainly with optical transitions to ground excitonic states as a tool to describe polarization-sensitive photoluminescence (PL) experiments.[1,2] Here, motivated by our progress in performing resonant PL excitation (PLE) spectroscopy, using one- and two-laser sources, we use the same model to consider transitions from various other levels. First, we consider transitions which result from the resonant absorption of one photon. Then, we add a second photon, resonantly tuned to the resonances of the optically excited QD. Since, as we explain below, the situation in this case is much richer than for PL only, we have to modify the notation for describing the QD many-carrier states. We use the following notation: A single-carrier state is described by its envelope wave function or orbital mode (O = 1,2, . . . ,6), where the number represents the energy order of the level so that O = 1 represents the ground state. O is followed by the type of carrier, electron (e) or heavy hole (h), and a superscript which describes the occupation of the single-carrier state. The superscript can be either 1 (open shell) or 2 (closed shell), subject to the Pauli exclusion principle (nonoccupied states are not described). All the occupied states of carriers of the same type are then marked by subscripts which describe the mutual spin configuration (σ) of these states.

A. Characterization of excitonic resonances

The ground exciton state $[X^0_{1,1} \equiv (1e^1)(1h^1)]$ is a two-carrier state, formed mainly by one electron and one heavy hole in their respective ground states. The exchange interaction between the electron and the heavy hole[2,14,15] is described, using the method of invariants,[16] by the following spin Hamiltonian:[14]

$$H_{X^0_{1,1}} = \sum_{i=x,y,z} \left(a_i^{1,1} S_i J_i + b_i^{1,1} S_i J_i^3\right), \tag{3}$$

where S_i (J_i) denotes the ith Cartesian component of the electron (hole) spin, and $a_i^{1,1}$ and $b_i^{1,1}$ are spin-spin coupling constants. The total spin projection on the ith direction is thereby given by $F_i = S_i + J_i$. Here as well, the interaction with light holes is neglected so that in J_i only heavy-hole spins are considered.[14] In matrix form, for the basis $|S_z\rangle \otimes |J_z\rangle$,

$$\begin{aligned} |-1/2,3/2\rangle &= \downarrow^1 \Uparrow^1, & F_z &= 1, \\ |1/2,-3/2\rangle &= \uparrow^1 \Downarrow^1, & F_z &= -1, \\ |1/2,3/2\rangle &= \uparrow^1 \Uparrow^1, & F_z &= 2, \\ |-1/2,-3/2\rangle &= \downarrow^1 \Downarrow^1, & F_z &= -2, \end{aligned} \tag{4}$$

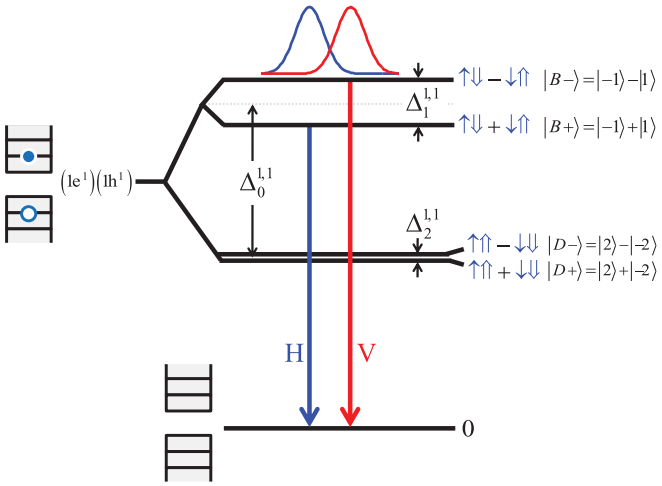

FIG. 1. (Color online) Schematic description of the energy levels of the $(1e^1)(1h^1)$ exciton and the allowed optical transitions from its states to the vacuum. The major parts of the spin wave functions are described to the right of each level. $\uparrow$ ($\Downarrow$) represents an electron (hole) with spin up (down) and a blue arrow represents a carrier in its first level. A blue (red) vertical arrow represents linearly polarized optical transition along the major (H) [minor (V)] axis of the QD. The bracketed numbers stand for the total spin projection of the carriers along the QD growth direction.

where $\uparrow^j$ ($\Downarrow^j$) indicates spin up (down) electron (heavy hole) in the orbital j; the Hamiltonian is given by

$$H_{X^0_{1,1}} = \frac{1}{2}\begin{pmatrix} & 1 & -1 & 2 & -2 \\ 1 & \Delta_0^{1,1} & \Delta_1^{1,1} & 0 & 0 \\ -1 & \Delta_1^{1,1} & \Delta_0^{1,1} & 0 & 0 \\ 2 & 0 & 0 & -\Delta_0^{1,1} & \Delta_2^{1,1} \\ -2 & 0 & 0 & \Delta_2^{1,1} & -\Delta_0^{1,1} \end{pmatrix}, \tag{5}$$

where $\Delta_0^{1,1} = 3(a_z^{1,1} + 2.25 b_z^{1,1})$, $\Delta_1^{1,1} = 1.5(b_x^{1,1} - b_y^{1,1})$, and $\Delta_2^{1,1} = 1.5(b_x^{1,1} + b_y^{1,1})$[14]. $\Delta_{0,1,2}^{1,1}$ are three constants, which fully characterize the exchange interaction between the carriers in the ground states.[16] It is clearly seen that in a C_{2v} symmetry the exchange interaction completely removes the degeneracy between the four possible various combinations of the electron-hole pair spin states.[10] The eigenenergies and the eigenstates are schematically described in Fig. 1. The lowest energy state is the symmetric dark exciton state which in our notation is described as follows: $|X^0_{1,1,D_+}\rangle \equiv \frac{1}{\sqrt{2}}[(1e^1)_{1/2}(1h^1)_{3/2} + (1e^1)_{-1/2}(1h^1)_{-3/2}]$. $\Delta_2^{1,1}$ above it lies the antisymmetric dark exciton state: $|X^0_{1,1,D_-}\rangle \equiv \frac{1}{\sqrt{2}}[(1e^1)_{1/2}(1h^1)_{3/2} - (1e^1)_{-1/2}(1h^1)_{-3/2}]$. $\Delta_2^{1,1}$ is known to be quite small and believed to be orbit independent.[16] It was recently measured from the temporal period of the coherent precession of the dark exciton spin to be 1.4 μeV.[17] The bright exciton eigenstates in which the electron and heavy-hole spins are antialigned lie $\Delta_0^{1,1}$ above the dark exciton states. The isotropic e-h exchange $\Delta_0^{1,1}$ was previously found to be about 300 μeV by magneto-optical measurements.[18]

The symmetric and antisymmetric bright exciton states $|X^0_{1,1,B\pm}\rangle \equiv \frac{1}{\sqrt{2}}[(1e^1)_{-1/2}(1h^1)_{3/2} \pm (1e^1)_{1/2}(1h^1)_{-3/2}]$

are split by the anisotropic e-h exchange $\Delta_1^{1,1}$. The magnitude and sign of $\Delta_1^{1,1} = -34\ \mu$eV is directly measured by polarization-sensitive PL spectroscopy. Since $\Delta_1^{1,1}$ is negative, the antisymmetric state ($|X^0_{1,1,B-}\rangle$) is higher in energy than the symmetric one ($|X^0_{1,1,B+}\rangle$).[2,15]

Conservation of angular momentum dictates that when a $\downarrow\Uparrow$ ($\uparrow\Downarrow$) e-h pair radiatively recombines, a right- (left-) hand circularly polarized photon is emitted. It follows that radiative recombination from the symmetric (antisymmetric) bright exciton state is linearly polarized H (V) along the major (minor) in-plane axis of the QD.[16,19] We note that the symmetric and antisymmetric dark and bright exciton states are by no means unique to the first single-carrier spatial levels (Oe = Oh = 1). In fact, similar bright and dark excitonic states are formed for any combination of Oe and Oh single-carrier states. In general, $\Delta_{0,1,2}^{\mathrm{Oe,Oh}}$ depend on the orbital mode of the carriers.[2,15]

When the laser is resonantly tuned into one of the excited bright exciton states and its light is polarized correctly, the light is absorbed and a single electron-hole pair is photogenerated. For example, let us consider the states $|X^0_{1,2,B\pm}\rangle \equiv 1/\sqrt{2}[(1e^1)_{-1/2}(2h^1)_{3/2} \pm (1e^1)_{1/2}(2h^1)_{-3/2}]$. These states are similar to the ground bright states $|X^0_{1,1,B\pm}\rangle$, albeit here the hole is in its second orbital mode (Oh = 2). The electron and hole pair will be photogenerated in these levels, and then the hole will rapidly relax nonradiatively (within ~20 psec[20,21]), by emitting phonons, to the ground level (Oe = Oh = 1). This relaxation is faster than the radiative recombination rate (~1 nsec).

Experimental identification of single-photon or single-exciton transitions is conventionally done by polarization-sensitive PL and PLE spectroscopies. In PL, a QD is optically excited. The excitation gives rise to light emission from various long-lived states which do not relax to lower energy states within their radiative lifetime. Polarization- and intensity-sensitive PL spectroscopies are in particular useful for these identifications. For example, the bright exciton typically gives rise to a PL doublet composed of two cross-linearly polarized components. These components are due to recombination from each of its nondegenerate eigenstates.

The second orbital wave function (p_H) has one node along the major symmetry axis of the QD. As a result $\Delta_1^{1,2}$ is positive and therefore the symmetric eigenstate $|X^0_{1,2,B+}\rangle$ is higher in energy than the antisymmetric eigenstate.[15] It thus follows that the V linearly polarized transition to this exciton is lower in energy than the H polarized one. When the $|X^0_{1,2,B-}\rangle$ ($|X^0_{1,2,B+}\rangle$) state is excited, the hole rapidly relaxes nonradiatively to its ground state, releasing its energy into acoustical phonons. Since phonons do not interact with the carriers' spin,[8,20,21] the spin wave function's symmetry remains the same, and the recombination occurs from the $|X^0_{1,1,B-}\rangle$ ($|X^0_{1,1,B+}\rangle$) state. Thus, polarization-sensitive PLE spectroscopy can be efficiently used to identify and sort various excitonic resonances.

B. Characterization of biexcitonic resonances

The ground biexciton state is formed mainly by two spin-paired electrons and two spin-paired heavy holes in their respective ground states. In our notation this state is described as follows: $|XX^0_{1,1,1,1}\rangle \equiv (1e^2)(1h^2)$. We note that spin-paired carriers can only form an antisymmetric spin singlet state and therefore the σ subscript in this case is redundant and is omitted from the pair's state description. For unpaired carriers, however, the situation is different. Two unpaired carriers can form either one antisymmetric singlet state or three symmetric triplet states. Therefore, in this case we do assign σ subscripts for describing the unpaired carriers' wave functions. For two unpaired carriers the σ can either be S, to indicate a singlet state, or T_m, to indicate a triplet state. Here m is the total spin projection, 0 or ±1 (0 or ±3) of the pair of electrons (heavy holes), along the QD growth direction. A full description of a state with two unpaired electrons and two unpaired holes has therefore the form

$$\left|XX^0_{\mathrm{O_{e1},O_{e2},O_{h1},O_{h2},\sigma_e,\sigma_h}}\right\rangle \equiv (\mathrm{O_{e1}e^1O_{e2}e^1})_{\sigma_e}(\mathrm{O_{h1}h^1O_{h2}h^1})_{\sigma_h}. \quad (6)$$

We note that for a given set of 4 unpaired spatial coordinates, 16 different states with different spin configurations are possible. These are naturally divided into the following 4 subgroups: one state, similar in nature to the ground biexciton state, in which the two electrons form a singlet (e-singlet) and the two heavy holes also form a singlet (h-singlet); three states in which the electrons form an e-singlet and the holes a triplet (h-triplet); three in which the holes form an h-singlet and the electrons an e-triplet; and nine in which both the electrons and holes form triplets (e-triplet–h-triplet). These four subgroups have different energies due to the exchange interactions between carriers of the same charge. The lowest energy level includes the 9 e-triplet–h-triplet states, the two intermediate groups include the 6 e-triplet–h-singlet and e-singlet–h-triplet states, and the highest energy one includes only a single e-singlet–h-singlet state.

For simplicity, we begin by characterizing optical transitions in which at least one type of carrier forms a singlet. In Fig. 2 we schematically describe the energy levels and the spin

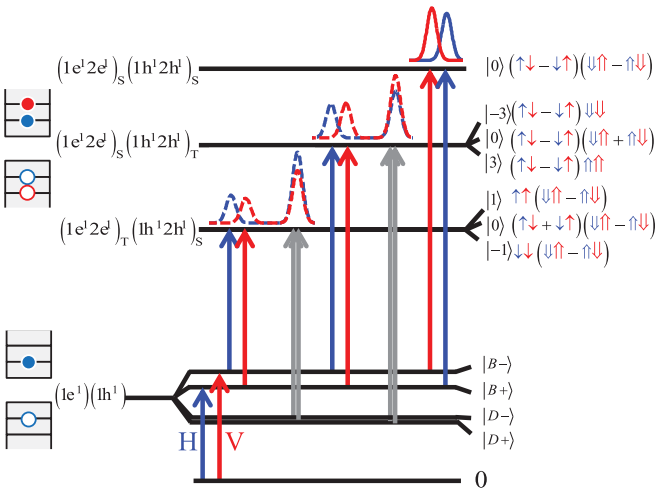

FIG. 2. (Color online) Schematic description of the energy levels and spin wave functions of the configuration $(1e^1 2e^1)_{\sigma_e}(1h^1 2h^1)_{\sigma_h}$, for $(\sigma_e,\sigma_h) = (T,S),(S,T),(S,S)$. The notations are as in Fig. 1. Calculated two-laser PLE spectra are presented by dashed (solid) lines for cross-linearly (co-linearly) polarized exciton and biexciton transitions. Blue (red) lines represent H (V) polarized biexcitonic transitions.

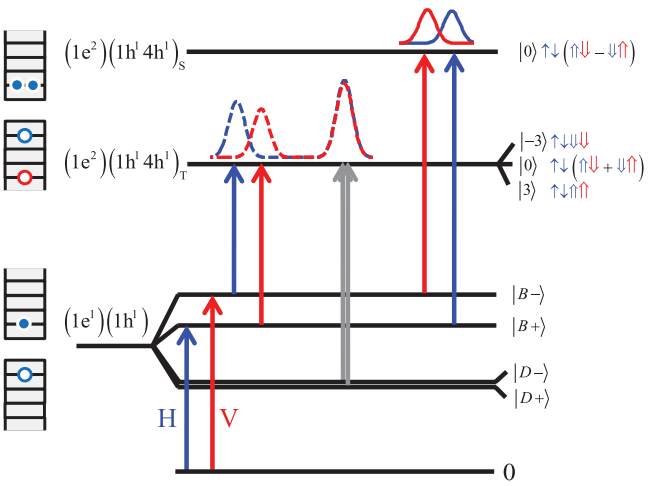

FIG. 3. (Color online) Schematic description of the energy levels and spin wave functions of the configuration $(1e^2)(1h^1 4h^1)$. The major parts of the spin wave functions are described to the right of each level. The notations are as in Fig. 1, where $\uparrow$ ($\Downarrow$) represents an electron (hole) with spin up (down) and a blue (red) arrow represents a carrier in its first (excited) level. Calculated two-laser PLE spectra are presented by dashed (solid) lines for cross-linearly (co-linearly) polarized excitonic and biexcitonic transitions. Blue (red) lines represent H (V) polarized biexcitonic transitions.

wave functions of the configuration $(1e^1 2e^1)_{\sigma_e}(1h^1 2h^1)_{\sigma_h}$, for the cases $(\sigma_e,\sigma_h) = (T,S),(S,T)$, or (S,S). The major parts of the spin wave functions are described to the right of each level, where $\uparrow$ ($\Downarrow$) represents an electron (hole) with spin up (down) and a blue (red) arrow represents a carrier in its first (second) level. The bracketed numbers stand for the total spin of the configuration. H (V) polarized optical transitions are represented by blue (red) vertical arrows.

We note that singlet-triplet and singlet-singlet biexcitonic resonances may, in principle, occur also when the two carriers that form the singlet reside in the same single-carrier orbital mode (the two carriers are paired). Naive intuitive considerations, which are based on single-band models, predict that these transitions should be weak, due to the small spatial overlap between the electron and hole orbital modes which belong to different O numbers.[22] Transitions which involve orbital modes of different symmetries should be forbidden in particular, since then, their dipole moment vanishes. Nevertheless, these optically forbidden transitions were previously observed in PLE spectroscopy of quantum wells[23] and QDs.[24,25]

In Fig. 3 we present an example for the case in which the electrons are paired in their ground single-carrier level while the holes are not. One hole is in the Oh = 1 *s*-like orbital and the other is in the Oh = 4, d_{HH}-like orbital. Since the electrons here are paired, they form a singlet; thus their total spin vanishes. Therefore, the e-h exchange interaction is not expected to remove the degeneracy between the holes' triplet states. We find, however, that this degeneracy is slightly removed due to many-carrier mixing effects. Previous works attributed this effect to anisotropic h-h exchange interactions,[1,24] which our model does not contain.

Turning to Fig. 2 again, we note that two absorption resonances are expected from the bright exciton states into an e-singlet-h-singlet state. These two transitions form a typical cross-linearly polarized doublet, resembling the optical transitions from the vacuum to the bright exciton states (see Fig. 1). Four transitions are excepted from the exciton states into the three e-singlet–h-triplet states, and four similar ones into the e-triplet–h-singlet states. Two of these four are cross-linearly polarized transitions from the bright exciton states into the state in which the two holes' (or electrons') spins are antiparallel (T_0), and two cross-linearly polarized transitions from each one of the dark exciton states into the corresponding symmetric and antisymmetric combinations of the parallel hole (or electron) spin states $T_{\pm 3}$ ($T_{\pm 1}$) of the biexciton. By inspecting the wave functions of the initial and final state of each optical transition one immediately sees that the oscillator strength of the optical transitions from the bright exciton states is exactly half that of the transitions from the dark exciton states. Moreover, since both the dark exciton and corresponding biexciton pair states are nearly degenerate, these two transitions form one unpolarized spectral line. Therefore, the total intensity of this line is four times larger than that of the other two transitions. The calculated spectra are presented in Fig. 2 and Fig. 3. In obtaining these spectra, the calculated transition energies are convoluted with normalized Gaussians of 50 μeV width, to take into account the finite lifetime of the spin-blockaded biexcitons. Transitions in which the exciton and biexciton photons are co-linearly (cross-linearly) polarized are presented by solid (dashed) lines, where blue (red) lines represent H- (V-) polarized biexciton photons.

We now turn to discuss the optical transitions into the e-triplet–h-triplet states. The electron-hole (e-h) exchange interactions, which in our QDs are typically about an order of magnitude smaller than same-carrier exchange interactions, remove the degeneracy between the states within this subgroup. We actually calculate the eigenenergies and eigenstates accurately using a CI model.[2,13] However, for a more intuitive discussion one can build an effective biexciton e-h exchange Hamiltonian for the subspace of $(1e^1 2e^1)_{\mathrm{T_e}}(1h^1 2h^1)_{\mathrm{T_h}}$, using the single exciton effective e-h exchange Hamiltonian of Eq. (3), such that an element is defined as follows:[26]

$$\begin{aligned} {}_f\langle J_z^2, J_z^1, S_z^2, S_z^1 | H_{XX^0_{1,2,1,2}} | S_z^1, S_z^2, J_z^1, J_z^2 \rangle_i \\ = {}_f\langle J_z^1, S_z^1 | H_{X^0_{1,1}} | S_z^1, J_z^1 \rangle_i \\ + {}_f\langle J_z^2, S_z^1 | H_{X^0_{1,2}} | S_z^1, J_z^2 \rangle_i \\ + {}_f\langle J_z^1, S_z^2 | H_{X^0_{2,1}} | S_z^2, J_z^1 \rangle_i \\ + {}_f\langle J_z^2, S_z^2 | H_{X^0_{2,2}} | S_z^2, J_z^2 \rangle_i, \end{aligned} \tag{7}$$

where $H_{X^0_{i,j}}$ is the single e-h pair spin Hamiltonian for electron and hole in the orbital modes i and j, respectively, and the subscript i (f) denotes the initial (final) spin state. We change to a new basis in which the same-carrier exchange states are diagonal. The weak e-h exchange interactions are then treated as perturbations on these states. A similar approach was previously used for describing charged excitons (trions).[27,28]

Taking only the subspace of the e-triplet–h-triplet spin states, $|\sigma_e\rangle \otimes |\sigma_h\rangle$,

$$
\begin{aligned}
|-1,3\rangle &= \downarrow^1\downarrow^2\Uparrow^1\Uparrow^2 \qquad F_z = 2,\\
|-1,0\rangle &= \downarrow^1\downarrow^2 \frac{(\Downarrow^1\Uparrow^2 + \Uparrow^1\Downarrow^2)}{\sqrt{2}} \qquad F_z = -1,\\
|-1,-3\rangle &= \downarrow^1\downarrow^2\Downarrow^1\Downarrow^2 \qquad F_z = -4,\\
|0,3\rangle &= \frac{(\uparrow^1\downarrow^2 + \downarrow^1\uparrow^2)}{\sqrt{2}}\Uparrow^1\Uparrow^2 \qquad F_z = 3,\\
|0,0\rangle &= \frac{(\uparrow^1\downarrow^2 + \downarrow^1\uparrow^2)(\Downarrow^1\Uparrow^2 + \Uparrow^1\Downarrow^2)}{2} \qquad F_z = 0,\\
|0,-3\rangle &= \frac{(\uparrow^1\downarrow^2 + \downarrow^1\uparrow^2)}{\sqrt{2}}\Downarrow^1\Downarrow^2 \qquad F_z = -3,\\
|1,3\rangle &= \uparrow^1\uparrow^2\Uparrow^1\Uparrow^2 \qquad F_z = 4,\\
|1,0\rangle &= \uparrow^1\uparrow^2 \frac{(\Downarrow^1\Uparrow^2 + \Uparrow^1\Downarrow^2)}{\sqrt{2}} \qquad F_z = 1,\\
|1,-3\rangle &= \uparrow^1\uparrow^2\Downarrow^1\Downarrow^2 \qquad F_z = -2,
\end{aligned}
\tag{8}
$$

we obtain the following matrix (neglecting many-body mixing corrections):

$$
H_{XX^0_{TT}} = \frac{1}{2}
\begin{array}{c|ccccccccc}
 & 2 & -1 & -4 & 3 & 0 & -3 & 4 & 1 & -2\\
\hline
2 & \widetilde{\Delta}_0 & 0 & 0 & 0 & \widetilde{\Delta}_1 & 0 & 0 & 0 & 0\\
-1 & 0 & 0 & 0 & \widetilde{\Delta}_2 & 0 & \widetilde{\Delta}_1 & 0 & 0 & 0\\
-4 & 0 & 0 & -\widetilde{\Delta}_0 & 0 & \widetilde{\Delta}_2 & 0 & 0 & 0 & 0\\
3 & 0 & \widetilde{\Delta}_2 & 0 & 0 & 0 & 0 & 0 & \widetilde{\Delta}_1 & 0\\
0 & \widetilde{\Delta}_1 & 0 & \widetilde{\Delta}_2 & 0 & 0 & 0 & \widetilde{\Delta}_2 & 0 & \widetilde{\Delta}_1\\
-3 & 0 & \widetilde{\Delta}_1 & 0 & 0 & 0 & 0 & 0 & \widetilde{\Delta}_2 & 0\\
4 & 0 & 0 & 0 & 0 & \widetilde{\Delta}_2 & 0 & -\widetilde{\Delta}_0 & 0 & 0\\
1 & 0 & 0 & 0 & \widetilde{\Delta}_1 & 0 & \widetilde{\Delta}_2 & 0 & 0 & 0\\
-2 & 0 & 0 & 0 & 0 & \widetilde{\Delta}_1 & 0 & 0 & 0 & \widetilde{\Delta}_0
\end{array},
\tag{9}
$$

where $\widetilde{\Delta}_0 = (\Delta_0^{Oe_1,Oh_1} + \Delta_0^{Oe_1,Oh_2} + \Delta_0^{Oe_2,Oh_1} + \Delta_0^{Oe_2,Oh_2})/4$ and $\widetilde{\Delta}_{1,2} = (\Delta_{1,2}^{Oe_1,Oh_1} + \Delta_{1,2}^{Oe_1,Oh_2} + \Delta_{1,2}^{Oe_2,Oh_1} + \Delta_{1,2}^{Oe_2,Oh_2})/8$. In Table I we present the nine eigenenergies and eigenfunctions of the effective Hamiltonian $H_{XX^0_{TT}}$. These eigenenergies and spin wave functions are also presented in Fig. 4. The allowed optical transitions between the ground exciton states to these biexciton states, together with their polarization selection rules, are presented as well. We note that since a photon can carry angular momentum of ± 1 only, biexciton resonances of total spin 3 and 1 can be reached optically only from the ground dark exciton states. Similarly, biexciton resonances of total spin 0 and 2 can be reached optically from the bright exciton states only. Biexciton states with total spin 4 cannot be reached optically.

C. Many-carrier mixing effects

The above discussion assumes that, to first order, the interactions between the carriers are much smaller in comparison with the single-carrier level separations. Therefore, we safely ignore contributions to the biexciton eigenstates which result from mixing with other configurations outside the subspace considered. Our model, however, does include these contributions,[2,13] and as we show below, in some cases, specifically when otherwise the transitions are forbidden, mixing with other configurations is directly observed in the experimental data.

TABLE I. Calculated eigenenergies and their respective spin configurations for the e-triplet–h-triplet states. The base states are expressed by their total spin projection $|F_z\rangle$.

Energy	Configuration
$-\widetilde{\Delta}_0$	$\|4\rangle - \|-4\rangle$
$-(\widetilde{\Delta}_1 + \widetilde{\Delta}_2)/2$	$(\|1\rangle + \|-1\rangle) - (\|3\rangle + \|-3\rangle)$
$-(\widetilde{\Delta}_1 - \widetilde{\Delta}_2)/2$	$(\|1\rangle - \|-1\rangle) - (\|3\rangle - \|-3\rangle)$
$(\widetilde{\Delta}_1 - \widetilde{\Delta}_2)/2$	$(\|1\rangle - \|-1\rangle) + (\|3\rangle - \|-3\rangle)$
$(\widetilde{\Delta}_1 + \widetilde{\Delta}_2)/2$	$(\|1\rangle + \|-1\rangle) + (\|3\rangle + \|-3\rangle)$
$\widetilde{\Delta}_0$	$-(\|2\rangle + \|-2\rangle)$
$R_i, i = 1,2,3$	
$R_1 \to [-\widetilde{\Delta}_0]$	$\to [\|4\rangle + \|-4\rangle]$
$R_2 \to [\widetilde{\Delta}_0 - \sqrt{\widetilde{\Delta}_0^2 + 2\widetilde{\Delta}_1^2}/2]$	$\to [\|0\rangle]$
$R_3 \to [\widetilde{\Delta}_0 + \sqrt{\widetilde{\Delta}_0^2 + 2\widetilde{\Delta}_1^2}/2]$	$\to [\|2\rangle + \|-2\rangle]$

[a] R_i is the ith root of the equation $2R_i^3 - (2\widetilde{\Delta}_0^2 + 2\widetilde{\Delta}_1^2 + \widetilde{\Delta}_2^2)R_i + \widetilde{\Delta}_0(\widetilde{\Delta}_2^2 - \widetilde{\Delta}_1^2) = 0$. The expressions in square brackets are obtained for the case $\widetilde{\Delta}_2 \ll \widetilde{\Delta}_1 \ll \widetilde{\Delta}_0$. R_i is given to order $(\widetilde{\Delta}_1/\widetilde{\Delta}_0)^2$.

Our model includes six orbital modes for each carrier. The many-carrier eigenstates are obtained by the diagonalization of the many-body Hamiltonian, which is constructed from all the possible configurations of the confined carriers in a system of six bound levels. Thus, a many-carrier eigenstate always contains contributions from different combinations of single-carriers' orbital modes.

An example for transitions in which these contributions become important are the optical transitions from the $(1e^12e^1)_{\sigma_e}(1h^2)$ biexciton to the first excited exciton state where the leading contribution comes from the configuration $(1e^1)(2h^1)$. Our model calculation resulted in optical transitions between these states, as indeed we found experimentally (see below). In Fig. 5 we describe the energy level structure

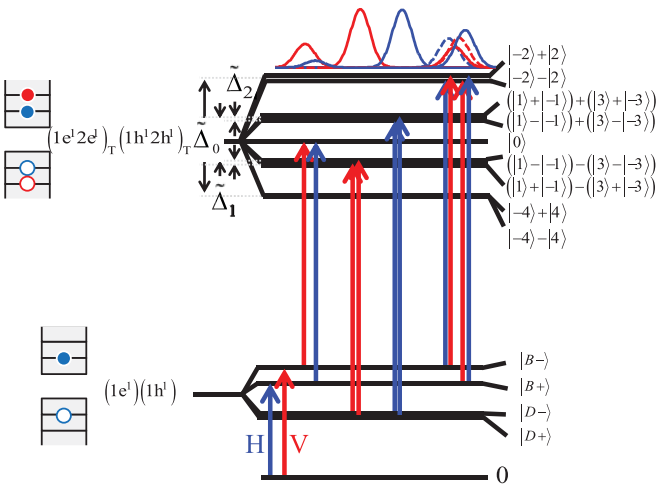

FIG. 4. (Color online) Schematic description of the energy levels of the $(1e^12e^1)_T(1h^12h^1)_T$ biexciton and their optical transitions. The major parts of the spin wave functions are described to the right of each level. A blue (red) vertical arrow represents linearly polarized optical transition along the major (H) [minor (V)] axis of the QD.

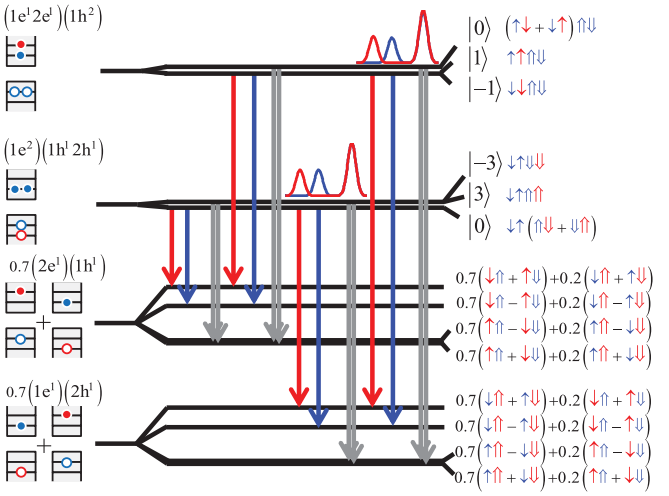

FIG. 5. (Color online) Schematic description of the energy levels of $(1e^2)(1h^12h^1)_T$ and $(1e^12e^1)_T(1h^2)$ biexcitons and the excited exciton states $(1e^1)(2h^1)$ and $(2e^1)(1h^1)$. The notations used here are the same as in Fig. 3. The curves describe calculated PL spectra of the transitions to the $(1e^1)(2h^1)$ excited excitons. The calculated transitions to the $(2e^1)(1h^1)$ excited excitons are not visible due to the short lifetime of the final state.

of the $(1e^2)(1h^12h^1)_T$ and $(1e^12e^1)_T(1h^2)$ biexcitons. Since these excited biexciton states are spin blockaded for thermal relaxation, they decay radiatively by recombination of a ground-state e-h pair. The optical transitions that originate from their decay are also described in Fig. 5. If one neglects mixing, it follows that the $(1e^2)(1h^12h^1)_T$ biexcitons decay into excited $(1e^1)(2h^1)$ excitons and the $(1e^12e^1)_T(1h^2)$ biexcitons decay into $(2e^1)(1h^1)$ excitons. These two excited excitons are, however, highly mixed due to the Coulomb interaction between the electron and the hole. Roughly speaking, our model shows that each biexciton group decays into both excited exciton states, resulting in four sets of three spectral lines. Each group of three spectral lines resembles the sets described in Fig. 2 and Fig. 3. It contains two lower energy cross-linearly polarized lines and one fourfold stronger unpolarized line. The calculated PL spectra which result from these transitions are presented in Fig. 5. The spectral width of the lines which result from emission to the lower energy excited exciton states [mainly $(1e^1)(2h^1)$] are obtained by convoluting the calculated transitions with Gaussians of $\sim$50 μeV, accounting for the finite lifetime of the excited hole states. Similarly, the spectral width of the lines which result from emission to the higher energy excited exciton states [mainly $(2e^1)(1h^1)$] should have been obtained by convolution with Gaussians of $\sim$1 meV (not visible, because the convolution results in a nearly uniform, unpolarized background on the relevant energy scale), due to the much shorter lifetime of the excited electron states. The difference between the two cases is due to the difference between the relaxation rates of the hole and the electron. While a hole in the second orbital state relaxes nonradiatively to the first orbital within $\sim$20 psec by emitting acoustical phonons,[20,21] the electron does so within less than 1 psec, by coupling to optical phonons.[29] The decay of the electrons is so rapid because the energy of optical phonons in the wetting layer nearly resonates with the energy separation between the two electronic orbitals ($\sim$29 meV[8]).

III. THE EXPERIMENTAL SETUP

The sample used in this work was grown by molecular-beam epitaxy on a (001) oriented GaAs substrate. One layer of strain-induced $In_xGa_{1-x}As$ QDs was deposited in the center of a one-wavelength microcavity formed by two unequal stacks of alternating quarter-wavelength layers of AlAs and GaAs, respectively. The height and composition of the QDs were controlled by partially covering the InAs QDs with a 3 nm layer of GaAs and subsequent growth interruption. To improve photon collection efficiency, the microcavity was designed to have a cavity mode which matches the QD emission due to ground-state e-h pair recombinations. During the growth of the QD layer the sample was not rotated, resulting in a gradient in the density of the formed QDs. The estimated QD density in the sample areas that were measured is 10^8 cm^{-2}; however, the density of QDs that emit in resonance with the microcavity mode is more than two orders of magnitude lower.[30] Thus, single QDs separated by few tens of micrometers were easily located by scanning the sample surface during PL measurements. Strong antibunching in intensity autocorrelation measurements was then used to verify that the isolated QDs are single ones and that they form single-photon sources.

The experimental setup that we used for the optical measurements is described in Fig. 6. The sample was placed inside a sealed metal tube immersed in liquid helium, maintaining a temperature of 4.2 K. A 60× microscope objective with numerical aperture of 0.85 was placed above the sample and used to focus the light beams on the sample surface and to collect the emitted PL. The majority of this work was performed with cw excitation. We used one tunable Ti:sapphire laser to scan the energy. A second Ti:sapphire laser was used

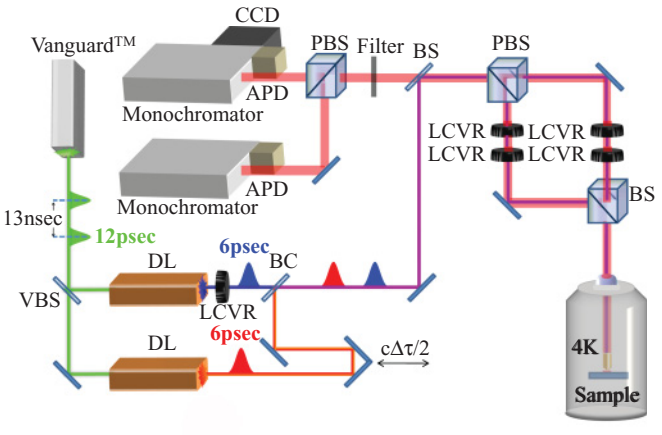

FIG. 6. (Color online) Schematic description of the experimental setup. The two dye laser pulses can be delayed one with respect to the other by a retroreflector mounted on a computer-controlled translation stage. For the cw experiments Ti:sapphire lasers were used. (P)BS stands for (polarizing) beam splitter, VBS for a variable beam splitter, BC for beam combiner, and LCVR for a liquid crystal variable retarder.

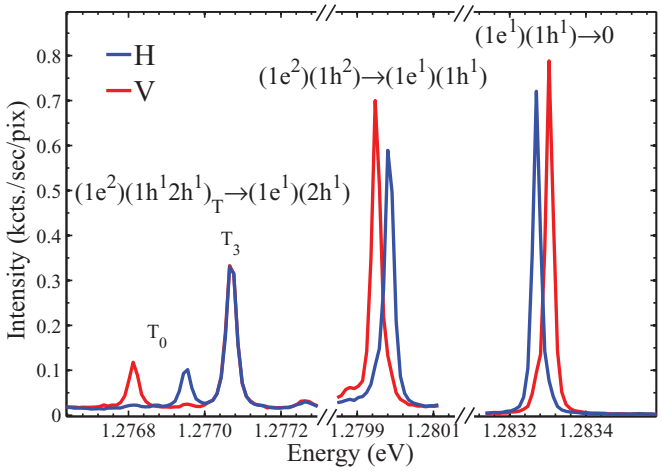

FIG. 7. (Color online) Linear-polarization-sensitive PL spectra, showing the neutral exciton and biexciton lines of a single QD excited by a 501 nm cw laser. The spectral transitions are identified in the figure.

for the two-photon excitation experiments. We performed also measurements with pulse excitation. In these measurements we used two dye lasers, synchronously pumped by the same frequency-doubled Nd:YVO_4 (Spectra Physics-Vanguard^{TM}) laser for generating the resonantly tuned optical pulses, as described in the figure. The repetition rate of the setup was 76 MHz, corresponding to a pulse separation of about 13 nsec. The duration of the laser pulses was about 6 psec and their spectral widths about 200 μeV. The delay between the pulses was controlled by a retroreflector on a translation stage.

The lasers' emission energy could have been continuously tuned using coordinated rotations of two plate birefringent filters and a thin etalon. The polarizations of the pulses were independently adjusted using a polarized beam splitter (PBS) and two pairs of computer-controlled liquid crystal variable retarders (LCVRs). The polarization of the emitted PL was analyzed by the same LCVRs and PBS. The PL was spectrally analyzed by a 1-meter monochromator and detected by either a silicon avalanche photodetector or by a cooled CCD camera.

In polarized PLE spectroscopy, one monitors the polarized emission from an identified PL line while varying the energy and polarization of the exciting light source. From the variations in the intensity of the emitted PL, one can readily identify many-carrier resonances in which the light is preferentially absorbed. Increased absorption, which results in increased emission intensity of a specific PL line, and its polarization sensitivity are then used to unambiguously identify the many-carrier state which forms a specific absorption resonance.[31,32]

IV. RESULTS

In Fig. 7 we present the polarization-sensitive PL spectrum of a single QD in resonance with the microcavity mode. The PL was obtained by exciting the QD with a 501 nm cw Ar+ laser. We found that at this excitation energy the QD is on average neutral.[21] The excitation intensity was roughly 1 W/cm^2 aiming at obtaining equal emission intensity from the exciton and biexciton lines.[33] The spectral neutral excitonic and biexcitonic lines which are relevant for this study are identified above the spectral features in the figure. We note that in addition to the ground bright exciton ($|X^0_{1,1,B\pm}\rangle$ to vacuum) and ground biexciton [$(1e^2)(1h^2)$ to $|X^0_{1,1,B\pm}\rangle$] lines, three additional biexcitonic lines are observed. These lines are due to recombination from the metastable biexciton configurations $(1e^2)(1h^12h^1)_T$ to the excited $(1e^1)(2h^1)$ exciton eigenstates. Two cross-linearly polarized lines are due to the transitions from the $(1e^2)(1h^12h^1)_{T_0}$ biexciton configuration to the excited bright exciton eigenstates, $|X^0_{1,2,B\pm}\rangle$, and one, unpolarized, is due to the (almost) degenerate transitions from the $(1e^2)(1h^12h^1)_{T_{\pm 3}}$ biexciton configurations to the excited dark exciton configurations, $|X^0_{1,2,D\pm}\rangle$. The observed emission intensity ratio of 1:1:4 is straightforward to understand,[21] as discussed above.

In Fig. 8 we present PLE spectra of the neutral excitonic and biexcitonic PL lines. Each panel in the figure presents the PLE spectrum of the PL spectral position marked by the vertical arrow on the expanded-scale PL spectrum to the left of the panel. This set of measurements, combined with additional measurements (discussed below) and the intuition that we gained from the model outlined above, allows us to resolve and identify most of the observed one- and two-photon resonances. The identified optical transitions are marked above the observed resonances.

A. Identification of excitonic lines

Figure 8(a) displays single-photon absorption resonances. When a photon is resonantly absorbed by the empty QD it enhances the emission from the exciton lines. The spectrum is dominated by the $(2e^1)(2h^1)$ absorption resonance. This excitonic state in which both the electron and the heavy hole are in their second p_H-like orbital mode is particularly strong due to the large overlap between the orbitals of the two carriers. The PLE spectrum contains additional, almost an order of magnitude weaker, sharp resonances. These resonances are due to "nondiagonal" excitonic states, in which the electron and the heavy hole differ in their orbital mode's symmetry. As a result, the spatial overlap between their modes is small and the oscillator strength for the optical transition is reduced. The nondiagonal transitions that we clearly identify are the $(1e^1)(6h^1)$ in which the electron is in its first, s-like orbital mode and the hole is in its d_{VV}-like modes. The oscillator strength for these transitions does not vanish, since there is some amount of overlap between the s-like and d_{VV}-like orbitals which are of even symmetry.[23]

More surprising is the observation of nondiagonal excitonic transitions between orbitals of different symmetries, like the $(1e^1)(2h^1)$. This transition, which is the lowest energy resonance in the exciton PLE spectrum, is unambiguously identified by its spectral position and spectral shape. As expected, it is a cross-linearly polarized doublet, with the same splitting and the same energy order of polarizations as the PL line due to the optical transition from the $(1e^2)(2h^11h^1)_{T_0}$ spin-blockaded biexciton to this $[(1e^1)(2h^1)]$ excited nondiagonal exciton state (Fig. 7). In both cases the spectral shape is dictated by the same final exciton states. Similarly, we identified the next in energy order doublet as the nondiagonal transitions to the bright levels of the $(1e^1)(3h^1)$ exciton. In these resonances $[(1e^1)(2h^1)$ and $(1e^1)(3h^1)]$, the electron is excited into the first,

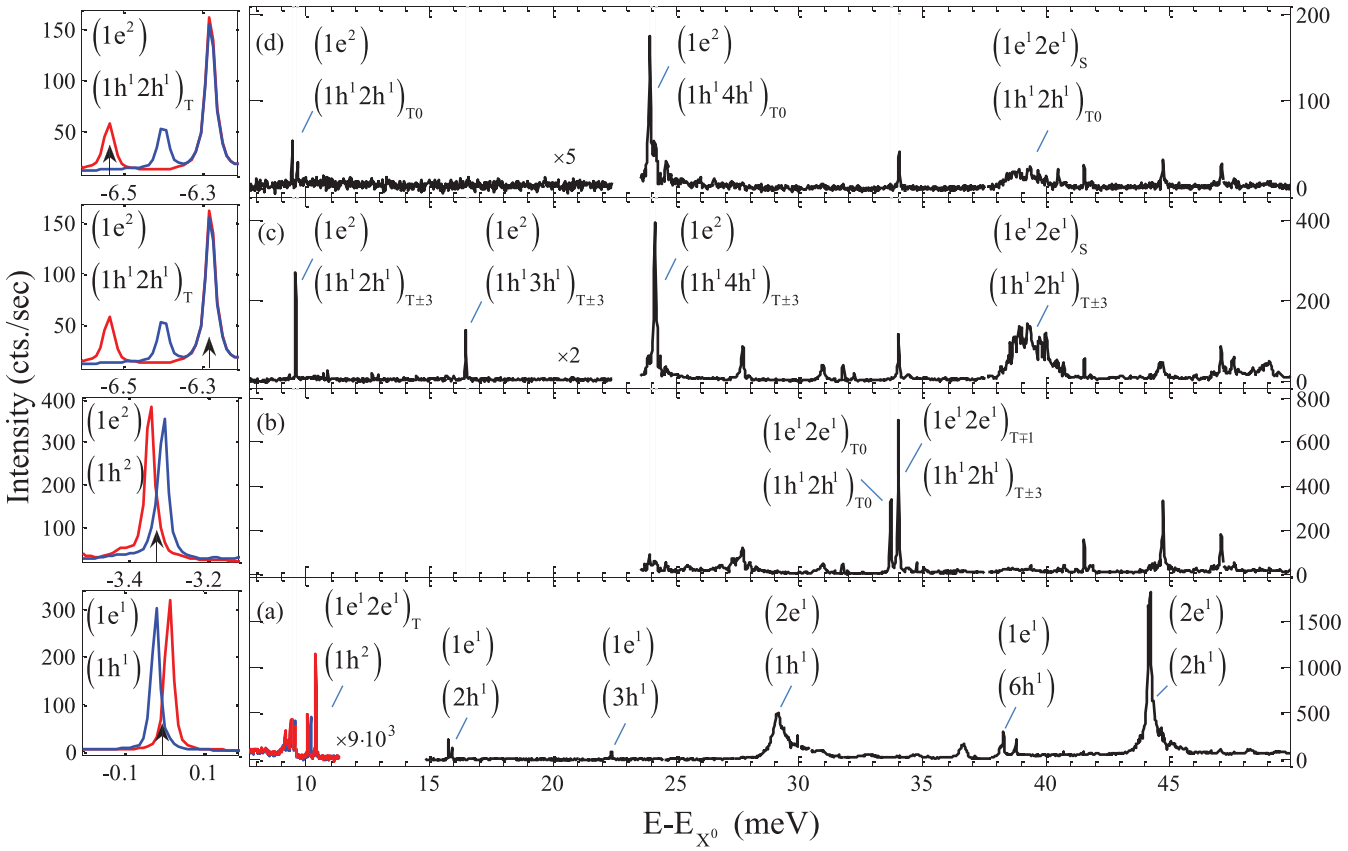

FIG. 8. (Color online) Linearly polarized PL spectra [left panels and the lower energy region in (a)] and PLE spectra (right panels) of a single QD. The PLE in (a) is measured by continuous scan of one laser's emission energy. The PLE spectra in (b)–(d) are measured with one laser's energy tuned to the excitonic resonance at 29 meV as shown in (a), while the energy of the second laser is continuously scanned. The PL line monitored in each case is marked on the corresponding left panel by a vertical black arrow. The assignment of the measured resonances is given by the state, which the QD is excited to, above each resonance.

s-like, symmetric orbital mode, while the hole is excited into the second, p_H-like, and third, p_V-like, antisymmetric mode, respectively. These optical transitions are therefore expected to be forbidden since the orbital modes' overlap vanishes. Their appearance indicates some symmetry breaking, possibly resulting from mixing with other bands.[24,25]

Another important mechanism which permits these symmetry-forbidden transitions is provided by phonon-induced mixing. This mixing is particularly strong when the phonon energy resonates with the single carrier's energy levels separation.[29] Clear evidence for such type of mixing-induced excitation is seen in the spectrally broad resonance 29 meV above the exciton line. This energy separation characterizes the energy of LO phonons in compounds of GaAs and InAs.[34–37] The $In_xGa_{1-x}As$ optical phonon closely resonates with the 1e-2e energy levels separation, resulting in an enhanced absorption in this spectral domain. This observation is also supported by the fact that the $(2e^1)(2h^1)$ resonance is higher in energy by about 29 meV from the $(1e^1)(2h^1)$ resonance, as expected.

B. Identification of biexcitonic lines

In Figs. 8(b)–8(d) PLE spectra of the biexcitonic lines are presented. During these measurements one laser was tuned to the broad excitonic resonance at 29 meV, thereby populating the QD with a bright exciton. The second laser energy was then continuously varied while the emission from one of the biexciton lines was monitored.

The PLE spectrum of the ground biexciton doublet, $(1e^2)(1h^2) \longrightarrow (1e^1)(1h^1)$, is presented in Fig. 8(b). The allowed transitions from the bright exciton states (total spin ±1) into the e-triplet–h-triplet biexciton states, $(1e^12e^1)_{T_0}(1h^12h^1)_{T_0}$ (total spin zero) and $(1e^12e^1)_{T_{\pm1}}(1h^12h^1)_{T_{\mp3}}$ (total spin ±2) are clearly observed, dominating, as expected, this spectrum.

In Fig. 8(c) the PLE is monitored by the PL line which corresponds to the decay of the spin-blockaded metastable biexciton, $(1e^2)(1h^12h^1)_{T_{\pm3}}$, by recombination of a ground e-h pair, to the excited dark exciton states, $|X^0_{1,2,D\pm}\rangle$. This PLE spectrum is dominated by e-singlet–h-triplet resonances, just like the resonance from which the light is monitored. The absorption resonance transitions from the ground dark exciton $|X^0_{1,1,D\pm}\rangle$ directly to the monitored resonance $[(1e^2)(1h^12h^1)_{T_{\pm3}}]$, by photogeneration of an Oe = 1 Oh = 2 e-h pair, is clearly identified as the lowest energy resonance in this PLE spectrum. Likewise, the resonances in which the hole is excited into the Oh = 3 and Oh = 4 orbitals $[(1e^2)(1h^13h^1)_{T_{\pm3}}$ and $(1e^2)(1h^14h^1)_{T_{\pm3}}$, respectively] are clearly identified as well. Photogenerated holes in these resonances nonradiatively

relax to the Oh = 2 level, where recombination occurs, since further nonradiative relaxation is spin blockaded.[20,21]

In addition, a broad resonance is observed ∼29 meV above the $(1e^2)(1h^12h^1)_{T_{\pm3}}$ biexciton resonance. This resonance is due to absorption into the $(1e^12e^1)_S(1h^12h^1)_{T_{\pm3}}$. This state is strongly coupled to the $(1e^2)(1h^12h^1)_{T_{\pm3}}$, by a one LO phonon, in a similar way to the coupling between the $(2e^1)(1h^1)$ and the $(1e^1)(1h^1)$ bright exciton states [Fig. 8(a)].

Similar spectral features are observed in Fig. 8(d) where the PLE is monitored through the decay of the metastable biexciton $(1e^2)(1h^12h^1)_{T_0}$ to the excited bright exciton state $|X^0_{1,2,B+}\rangle$. In this spectrum the absorption resonances from the bright exciton states to the $(1e^2)(1h^12h^1)_{T_0}$ and the $(1e^2)(1h^14h^1)_{T_0}$ states are identified. The weaker resonant absorption into the $(1e^2)(1h^13h^1)_{T_0}$ state is missing from this spectrum due to poor signal to noise ratio.

We note that the energy difference between the optical transitions $(1e^1)(1h^1) \longrightarrow (1e^2)(1h^12h^1)_{T_0}$ and $(1e^2)(1h^12h^1)_{T_0} \longrightarrow (1e^1)(2h^1)$ is 15.7 meV. As expected, this difference exactly matches the energy of the optical transition from the vacuum into the first excited exciton state $(1e^1)(2h^1)$.

The transitions to the states $(1e^2)(1h^12h^1)_{T_m}$ which are clearly observed in Fig. 8(c) and 8(d) are absent from the PLE spectrum of the ground biexciton [Fig. 8(b)]. This is due to the fact that in these cases the emitting state is directly excited and no intermediate nonradiative relaxation process is required. This is not the case when the $(1e^2)(1h^14h^1)_{T_0}$ state is excited. Here, since nonradiative relaxation of the hole must occur prior to the recombination, the resonance is weakly observed in the PLE spectrum of the ground biexciton state, as well. This means that in the relaxation process of the hole from the Oh = 4 to the Oh = 2 orbital state, its spin may slightly scatter.[20] Last, we note that the resonances $(1e^12e^1)_{T_{\pm1}}(1h^12h^1)_{T_{\mp3}}$ and $(1e^12e^1)_{T_0}(1h^12h^1)_{T_0}$ which are due to optical transitions from the bright exciton states are only observed in the PLE spectrum of the ground biexciton state [Fig. 8(b)]. Similarly, the resonances $(1e^12e^1)_{T_{\pm1}}(1h^12h^1)_{T_0}$ and $(1e^12e^1)_{T_0}(1h^12h^1)_{T_{\pm3}}$ which are due to optical transitions from the dark exciton states are only observed in PLE spectra of the spin blockaded biexcitons [Fig. 8(c) and 8(d)]. We note, however, that the bright exciton resonances $(1e^12e^1)_{T_{\pm1}}(1h^12h^1)_{T_{\mp3}}$ spectrally overlap with the dark exciton resonances $(1e^12e^1)_{T_{\pm1}}(1h^12h^1)_{T_0}$ and $(1e^12e^1)_{T_0}(1h^12h^1)_{T_{\pm3}}$, and therefore their final identification is also based on polarization-sensitive and time-resolved spectroscopy, as explained below.

In Fig. 9, we present examples of the use of polarization-sensitive spectroscopy as a tool for verifying the identity of the observed spectral resonances. The PLE resonances as monitored by the four biexcitonic PL transitions and by the ground exciton state are displayed in the figure for various combinations of rectilinear polarizations of the exciting two lasers and the detected PL. Since the figure describes e-singlet–h-triplet resonances, the experimentally measured optical transitions and their polarization selection rules can be directly compared with the theoretical expectations outlined in Fig. 3. The characteristic three-line structure of the optical transition into the e-singlet–h-triplet state is clearly resolved in Fig. 9. The lowest energy biexcitonic doublet is cross-linearly polarized, since each component is due to excitation of

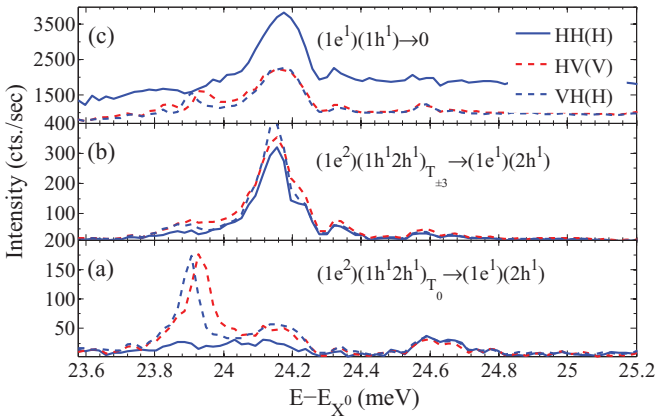

FIG. 9. (Color online) Expanded-energy-scale presentation of the two-laser polarization-sensitive PLE spectra revealing the optical transitions into the biexcitonic resonances $(1e^2)(1h^14h^1)_T$. The spectra are monitored by the PL lines of the transitions from the metastable biexcitons $(1e^2)(1h^12h^1)_{T_0}$ (a) and $(1e^2)(1h^12h^1)_{T_{\pm3}}$ (b) to the excited exciton $(1e^1)(2h^1)$ and the PL doublet of the transitions from the ground-state exciton $(1e^1)(1h^1)$ to the vacuum (c). Various rectilinear polarizations of the exciting lasers and the detected PL light are used. The first letter denotes the polarization of the laser tuned to the exciton resonance, the second, that to the biexciton, and the third, in parentheses, that of the detected emission. The two cross-polarized curves in the ground-state exciton (c) are multiplied by 3.

a different bright exciton eigenstate. The high energy line is unpolarized, and its intensity is twice stronger (even in rectilinear polarization) since it gets contributions from the two optically allowed transitions of the dark exciton eigenstates.[17] We note in particular that the energy separation between the cross-linearly polarized components of the lower energy

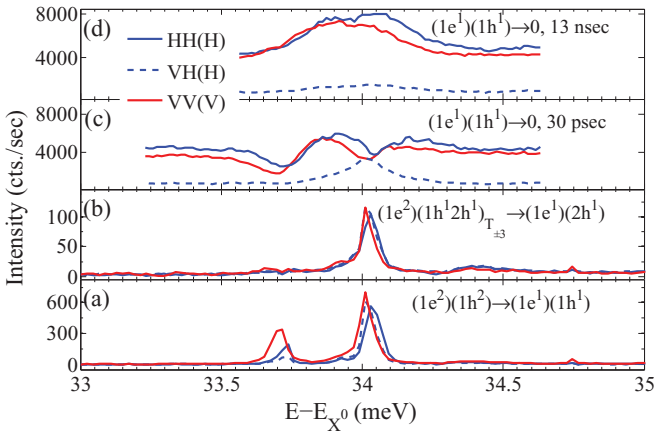

FIG. 10. (Color online) Expanded-energy-scale presentation of the two-color, polarization-sensitive PLE spectra revealing the optical transitions into the biexcitonic resonances $(1e^12e^1)_T(1h^12h^1)_T$. The spectra are monitored by the PL from the ground-state biexciton lines (a), the metastable biexciton $(1e^2)(1h^12h^1)_{T_{\pm3}}$ (b), and the ground-state exciton $(1e^1)(1h^1)$ with two pulsed lasers at 30 psec delay (c) and 13 nsec delay (d). Various rectilinear polarizations of the exciting lasers and the detected PL emission are used. The first letter denotes the polarization of the laser tuned to the exciton resonance, the second, that to the biexciton, and the third, in parentheses, that of the detected emission.

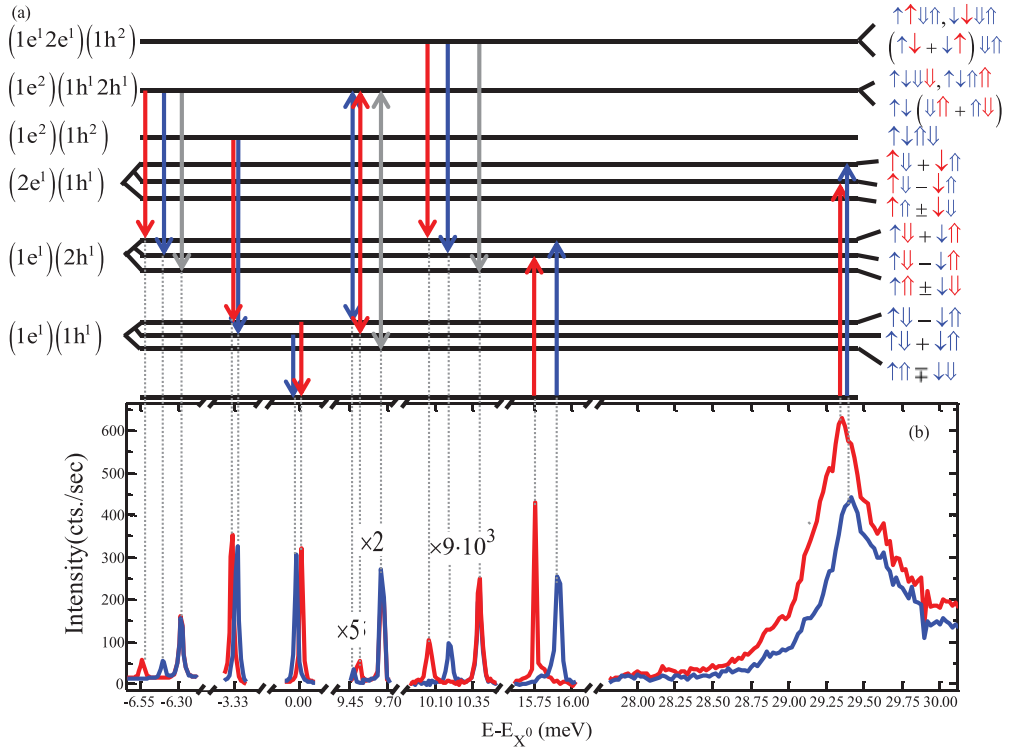

FIG. 11. (Color online) (a) Schematic description of the excitonic and biexcitonic energy levels and carriers' spin wave functions associated with the first and the second orbital modes. The optical transitions between these levels and in particular the "nondiagonal" ones are represented by vertical arrows. Blue (red) downward (upward) arrow describes horizontally (vertically) linearly polarized emission (absorption) transition. Gray arrows represent unpolarized transitions. The optical transitions in (a) are linked with the experimentally measured polarization-sensitive PL and PLE spectra in (b) and in (c), respectively. Solid blue (red) line represents horizontal (vertical) polarization.

doublet exactly matches as expected, that of the bright exciton (-34 μeV). The two-laser PLE spectrum of the ground-state exciton [Fig. 9(c)] reveals a striking difference between transitions from the bright exciton states and transitions from the dark ones. In the first type of transition population from the bright exciton is transferred into the biexciton state, in which polarization memory is totally lost, and thus the polarized PL emission is reduced. In the latter type population is transferred from the dark exciton into the bright exciton state due to the excitation to the biexciton state. Therefore, in this case the PL emission from the bright exciton states is enhanced.

In Fig. 10, we use similar methods for studying the richer spectrum of the e-triplet–h-triplet resonances. In this figure the optical transitions into the $(1e^1 2e^1)_T(1h^1 2h^1)_T$ biexciton states are studied and the experimentally measured transitions should be compared with the theoretical considerations outlined in Fig. 4. As can be seen in Fig. 4, there are six optical transitions from the bright exciton states into the e-triplet–h-triplet states, and four optical transitions from the dark exciton states. The lowest energy transitions are the cross-linearly polarized doublet due to optical transitions from the bright exciton states into the $(1e^1 2e^1)_{T_0}(1h^1 2h^1)_{T_0}$ biexciton. As mentioned above, this biexciton resonance is only observed in the PL from the ground biexciton states. For these optical transitions to occur, both lasers should be co-linearly polarized, as indeed the data show [Fig. 10(a)]. In addition there is a higher energy doublet due to the four optical transitions from the bright exciton states into the symmetric and antisymmetric biexciton states of total spin projection 2. Since these biexciton states are almost degenerate (in a similar way to the dark exciton states), the four transitions form an unpolarized doublet which is twice as strong as the lower energy cross-polarized one. Again, this is exactly what one sees in the polarization-sensitive PLE spectrum of the ground biexciton [Fig. 10(a)].

In Fig. 10(b) a strong resonance in the PLE spectrum of the PL line $(1e^2)(1h^1 2h^1)_{T_{\pm 3}}$ to $(1e^1)_{\pm 1/2}(2h^1)_{\pm 3/2}$ is observed. The resonances in this spectrum are expected to result mainly from excitations of the dark exciton states. As seen in Fig. 4, the optical transitions from the dark exciton states are expected to form a cross-linearly polarized doublet. Unfortunately, this doublet spectrally overlaps the unpolarized doublet due to transitions from the bright exciton states. We use time-resolved pulsed PLE spectroscopy in order to resolve these transitions.

In Fig. 10(c) we show two-pulse polarization-sensitive PLE spectra of the bright exciton lines when the temporal separation between the two pulses is relatively short (30 psec), while in Fig. 10(d) these spectra are shown for the case in which the temporal separation is 13 nsec. While in the first case, immediately after the photogeneration the exciton population is bright, in the second case only the dark exciton population lasts. The PLE spectroscopy reveals this fact in the following way: When the second pulse is tuned into a bright exciton to biexciton transition, the PL signal from the exciton lines is reduced, since from the biexciton state part of the population does not return to the monitored

TABLE II. Spectroscopically extracted e-h exchange interaction energies.

Energy Separation	Measured Value (μeV)
$\Delta_0^{1,1}$	123
$\Delta_1^{1,1}$	−34
$\Delta_0^{1,2}$	200
$\Delta_1^{1,2}$	151
$\Delta_1^{2,1}$	60
$\Delta_1^{2,2}$[a]	60

[a]Extracted from the $(2e^1)(2h^1)$ doublet and from the e-triplet–h-triplet resonances (see Fig. 4).

exciton state. This is particularly true for co-polarized pulses, since the polarization memory is lost in the biexciton states. Therefore, bright exciton transitions are seen as dips in the PLE spectrum of the exciton for co-polarized pulses and as peaks for cross-polarized pulses. Dark exciton transitions are always obtained as peaks in the PLE spectrum of the exciton, since they transfer dark populations into bright ones through the biexciton states. Thus, the polarized nature of the optical transitions from the dark exciton states into the $J = \pm 1, \pm 3$ biexciton states is clearly revealed in the polarization-sensitive PLE spectra of the exciton in Fig. 10(d).

C. The nondiagonal optical transitions

In Fig. 11 we focus our attention on the "nondiagonal" optical transitions that we identified in the PL and the one- and two-color PLE spectra. Only transitions which include p_H-like orbitals are considered. Figure 11(a) schematically describes the relevant excitonic and biexcitonic energy levels and the optical transitions between them, once the nondiagonal transitions become allowed. The (unnormalized) spin wave functions are described to the left of each level. Downward (upward) vertical arrows describe emission (absorption) and blue (red) stands for H (V) polarization. Gray arrows describe unpolarized transitions. We note that the transitions between the $(1e^2)(1h^12h^1)_T$ biexciton states and the $(1e^1)(1h^1)$ exciton states are observed both in PL and in PLE spectra.

The spectra are characterized by two repeating patterns: The first one is a cross-linearly polarized doublet. This doublet is due to the anisotropic e-h exchange induced splitting of the bright exciton states. In these doublets the symmetric state is lower (higher) in energy than the antisymmetric state for diagonal (nondiagonal) optical transitions. The second pattern has three spectral lines: a higher energy unpolarized line and a lower energy cross-linearly polarized doublet. This pattern is due to transitions from exciton to biexciton singlet-triplet states. The doublet is due to transitions from the bright exciton states and the unpolarized line is due to transitions from the dark exciton states. The optical transitions which are schematically described in Fig. 11(a) are linked to the experimentally measured transitions in the PL and in the PLE spectra [Fig. 11(b)].

TABLE III. The parameters used for the model.

Parameter	Value
$M^*_{\perp,h}$[a]	$0.25m_0$
M^*_e[a]	$0.065m_0$
l_h^x	53 Å
l_e^x	74 Å
$\xi = \frac{l_e^y}{l_e^x} = \frac{l_h^y}{l_h^x}$	0.87

[a]Reference 2.

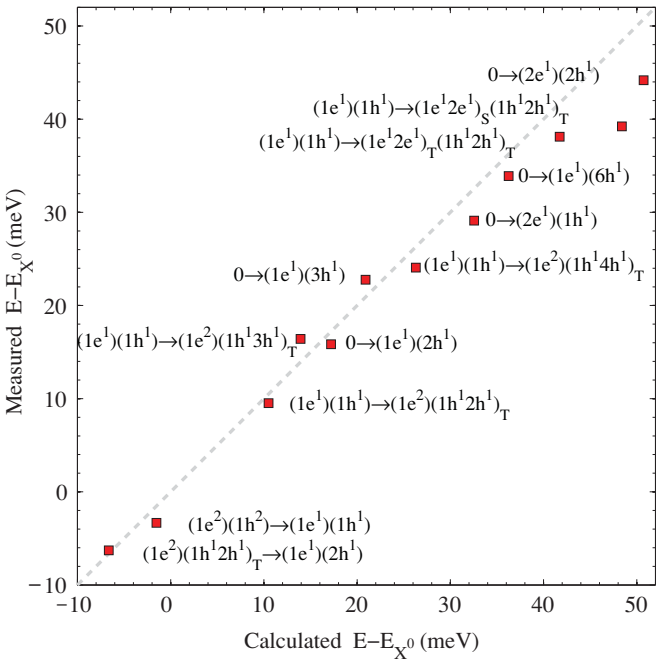

FIG. 12. (Color online) Comparison between the measured and calculated excitonic and biexcitonic transitions.

In Fig. 12 we compare between the measured excitonic and biexcitonic optical transitions and the calculated ones. Good agreement is achieved using the QD parameters listed in Table III. One notes that transitions which include the second single-electron state 2e deviate the most from the calculated ones. We believe that it is due to the optical phonon induced coupling between this state and the first electronic state. Our model does not consider this coupling.

Finally, we note that the three optical transitions from the $(1e^12e^1)_T(1h^2)$ to the $(1e^1)(2h^1)$ states are observed in the measured PL spectrum. This confirms our many-body description, as discussed in Sec. II C.

V. SUMMARY

In summary, we presented a comprehensive study of single, neutral semiconductor quantum dots subject to excitation by two variably polarized resonant excitations, one to exciton resonances, and the other to biexciton resonances. By monitoring the emission intensity from various exciton and

biexciton lines we completely characterize the rich one- and two-photon absorption spectra of single semiconductor quantum dots. The measured data are compared with a many-carrier theoretical model, based on simple, one-band parabolic potentials for electrons and heavy holes. While the model provides full understanding of the observed resonances, in terms of line shapes, energies, and polarization selection rules, it is short of quantitatively describing intensities of various "nondiagonal" optical transitions and spectral features which involve strong coupling with optical phonons. We believe that the understanding that our study provides should be very useful in applying semiconductor quantum dots as devices for quantum logical gates.

ACKNOWLEDGMENTS

The support of the US-Israel Binational Science Foundation (BSF), the Israeli Science Foundation (ISF), the Ministry of Science and Technology (MOST), Eranet Nano Science Consortium, and Technion's RBNI are gratefully acknowledged. We also acknowledge helpful discussions with Garnett Bryant.

*byael@tx.technion.ac.il

[1] M. Ediger, G. Bester, A. Badolato, P. M. Petroff, K. Karrai, A. Zunger, and R. J. Warburton, Nature Phys. **3**, 774 (2007).
[2] E. Poem, J. Shemesh, I. Marderfeld, D. Galushko, N. Akopian, D. Gershoni, B. D. Gerardot, A. Badolato, and P. M. Petroff, Phys. Rev. B **76**, 235304 (2007).
[3] P. Michler, A. Kiraz, C. Becher, W. V. Schoenfeld, P. M. Petroff, L. Zhang, E. Hu, and A. Imamoglu, Science **290**, 2282 (2000).
[4] P. Zanardi and F. Rossi, Phys. Rev. Lett. **81**, 4752 (1998).
[5] A. Imamoğlu, D. D. Awschalom, G. Burkard, D. P. DiVincenzo, D. Loss, M. Sherwin, and A. Small, Phys. Rev. Lett. **83**, 4204 (1999).
[6] D. Press, K. De Greve, P. L. McMahon, T. D. Ladd, B. Friess, C. Schneider, M. Kamp, S. Höfling, A. Forchel, and Y. Yamamoto, Nature Photonics **4**, 367 (2010).
[7] H. Kosaka, T. Inagaki, Y. Rikitake, H. Imamura, Y. Mitsumori, and K. Edamatsu, Nature (London) **457**, 702 (2009).
[8] Y. Benny, S. Khatsevich, Y. Kodriano, E. Poem, R. Presman, D. Galushko, P. M. Petroff, and D. Gershoni, Phys. Rev. Lett. **106**, 040504 (2011).
[9] D. P. DiVincenzo, Science **270**, 255 (1995).
[10] R. Singh and G. Bester, Phys. Rev. Lett. **104**, 196803 (2010).
[11] R. J. Warburton, B. T. Miller, C. S. Dürr, C. Bödefeld, K. Karrai, J. P. Kotthaus, G. Medeiros-Ribeiro, P. M. Petroff, and S. Huant, Phys. Rev. B **58**, 16221 (1998).
[12] A. Barenco and M. A. Dupertuis, Phys. Rev. B **52**, 2766 (1995).
[13] E. Dekel, D. Gershoni, E. Ehrenfreund, J. M. Garcia, and P. M. Petroff, Phys. Rev. B **61**, 11009 (2000).
[14] M. Bayer, G. Ortner, O. Stern, A. Kuther, A. A. Gorbunov, A. Forchel, P. Hawrylak, S. Fafard, K. Hinzer, T. L. Reinecke, S. N. Walck, J. P. Reithmaier, F. Klopf, and F. Schäfer, Phys. Rev. B **65**, 195315 (2002).
[15] T. Takagahara, Phys. Rev. B **62**, 16840 (2000).
[16] E. L. Ivchenko and G. E. Pikus, *Superlattices and other Heterostructures* (Springer-Verlag, Berlin, 1997).
[17] E. Poem, Y. Kodriano, C. Tradonsky, N. H. Lindner, B. D. Gerardot, P. M. Petroff, and D. Gershoni, Nature Phys. **6**, 993 (2010).
[18] S. Alon-Braitbart, E. Poem, L. Fradkin, N. Akopian, S. Vilan, E. Lifshitz, E. Ehrenfreund, D. Gershoni, B. D. Gerardot, A. Badolato, and P. M. Petroff, Physica E **32**, 127 (2006).
[19] D. Gammon, E. S. Snow, B. V. Shanabrook, D. S. Katzer, and D. Park, Phys. Rev. Lett. **76**, 3005 (1996).
[20] E. Poem, Y. Kodriano, C. Tradonsky, B. D. Gerardot, P. M. Petroff, and D. Gershoni, Phys. Rev. B **81**, 085306 (2010).
[21] Y. Kodriano, E. Poem, N. H. Lindner, C. Tradonsky, B. D. Gerardot, P. M. Petroff, J. E. Avron, and D. Gershoni, Phys. Rev. B **82**, 155329 (2010).
[22] G. Bastard, *Wave Mechanics Applied to Semiconductor Heterostructures* (Les Edition de Physique, Paris, 1990).
[23] R. C. Miller, A. C. Gossard, G. D. Sanders, Yia-Chung Chang, and J. N. Schulman, Phys. Rev. B **32**, 8452 (1985).
[24] T. Warming, E. Siebert, A. Schliwa, E. Stock, R. Zimmermann, and D. Bimberg, Phys. Rev. B **79**, 125316 (2009).
[25] E. Siebert, T. Warming, A. Schliwa, E. Stock, M. Winkelnkemper, S. Rodt, and D. Bimberg, Phys. Rev. B **79**, 205321 (2009).
[26] M. Z. Maialle and M. H. Degani, Phys. Rev. B **76**, 115302 (2007).
[27] K. V. Kavokin, Phys. Status Solidi (a) **195**, 592 (2003).
[28] I. A. Akimov, K. V. Kavokin, A. Hundt, and F. Henneberger, Phys. Rev. B **71**, 075326 (2005).
[29] S. Hameau, Y. Guldner, O. Verzelen, R. Ferreira, G. Bastard, J. Zeman, A. Lemaître, and J. M. Gérard, Phys. Rev. Lett. **83**, 4152 (1999).
[30] G. Ramon, U. Mizrahi, N. Akopian, S. Braitbart, D. Gershoni, T. L. Reinecke, B. Gerardot, and P. M. Petroff, Phys. Rev. B **73**, 205330 (2006).
[31] J. J. Finley, A. D. Ashmore, A. Lemaître, D. J. Mowbray, M. S. Skolnick, I. E. Itskevich, P. A. Maksym, M. Hopkinson, and T. F. Krauss, Phys. Rev. B **63**, 073307 (2001).
[32] M. E. Ware, E. A. Stinaff, D. Gammon, M. F. Doty, A. S. Bracker, D. Gershoni, V. L. Korenev, S. C. Badescu, Y. Lyanda Geller, and T. L. Reinecke, Phys. Rev. Lett. **95**, 177403 (2005).
[33] E. Dekel, D. V. Regelman, D. Gershoni, E. Ehrenfreund, W. V. Schoenfeld, and P. M. Petroff, Phys. Rev. B **62**, 11038 (2000).
[34] D. Sarkar, H. P. van der Meulen, J. M. Calleja, J. M. Becker, R. J. Haug, and K. Pierz, Phys. Rev. B **71**, 081302 (2005).
[35] D. Sarkar, H. P. van der Meulen, J. M. Calleja, J. M. Meyer, R. J. Haug, and K. Pierz, Appl. Phys. Lett. **92**, 181909 (2008).
[36] A. Lemaître, A. D. Ashmore, J. J. Finley, D. J. Mowbray, M. S. Skolnick, M. Hopkinson, and T. F. Krauss, Phys. Rev. B **63**, 161309 (2001).
[37] F. Findeis, A. Zrenner, G. Böhm, and G. Abstreiter, Phys. Rev. B **61**, R10579 (2000).